Extreme drought–accelerated dissolved carbon metabolism triggers pulsed CO_2 outgassing in karst lakes

Maofei Ni[1], Weijun Luo[2], Junbing Pu[3], Guangneng Zeng[1]*, Jinxiao Long[1], Jia Chen[2], Jing Zhang[3], Xiaodan Wang[1], Zhikang Wang[1]**

1. College of Eco-Environmental Engineering, Guizhou Minzu University, Guiyang 550025, China.

2. State Key Laboratory of Environmental Geochemistry, Institute of Geochemistry, Chinese Academy of Sciences, Guiyang, 550081, China

3. Karst Research Team, Chongqing Key Laboratory of Carbon cycle and Carbon regulation of Mountain Ecosystem, School of Geography and Tourism, Chongqing Normal University, Chongqing, 401331, China

*** Corresponding Author:**

Guangneng Zeng

Guizhou Minzu University (GMU)

Address: Guizhou Minzu University, Huaxi District, Guiyang City, Guizhou Province, P.R.China 550025

Email: augustinezeng@126.com

Zhikang Wang

Guizhou Minzu University (GMU)

Address: Guizhou Minzu University, Huaxi District, Guiyang City, Guizhou Province, P.R.China 550025

Email: wangzhikang@gzmu.edu.cn

Abstract

Karst aquatic ecosystems are important reservoirs of dissolved carbon (C), supporting dynamic CO_2 fluxes through the biological C pump. However, our current understanding of how sophisticated interactions between aquatic microbiomes and dissolved C turnover constrain the timing of CO_2 sequestration and emission remains limited. Here we capture an extreme drought event and the ensuing relatively wet conditions from systematic investigations in karst lakes, demonstrating that temporally distinct microbiomes are tuned to the metabolic patterns of dissolved C and thereby modulate CO_2 emissions. Specifically, we find that the extreme drought accelerates respiration of dissolved organic C, sharply increasing the CO_2 evasion rate. Wet conditions stimulate photosynthetic uptake of dissolved inorganic C, consuming lake CO_2 while promoting labile organic C formation. We therefore propose that during the observed extreme drought, pulses of CO_2 emissions from the study karst lakes occur after wet conditions end, as a consequence of rapid remineralization of newly produced bioavailable organic C~~, especially during extreme droughts~~. Our findings highlight the crucial importance of managing periodic CO_2 outgassing from karst waters under drought conditions for the implementation of region-specific C neutrality strategies.

Keywords: Karst waters, aquatic microbiome, dissolved carbon, CO_2 flux, extreme drought

Graphical Abstract

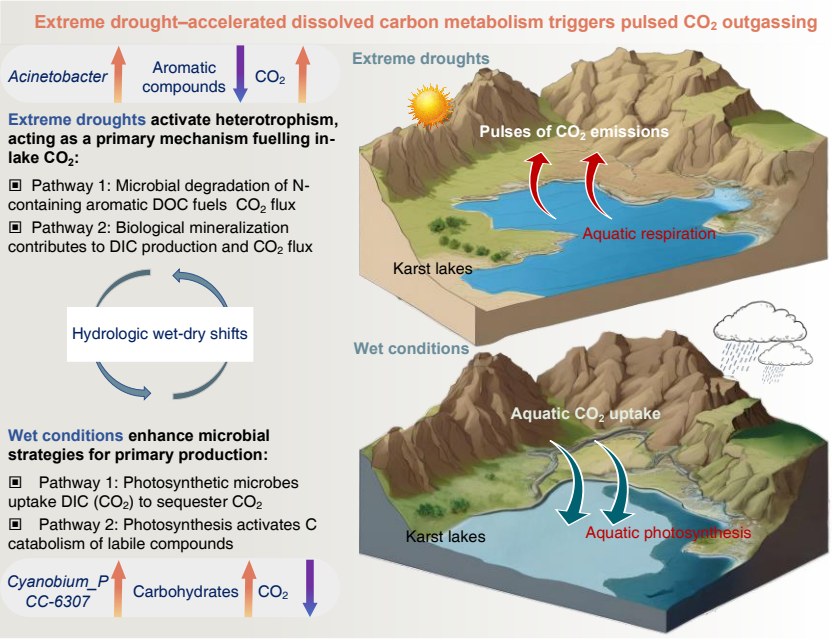

1. Introduction

Lakes store, metabolize and release large quantities of natural carbon (C), representing a funnel of aquatic C budget (Bogard et al., 2019; Borges et al., 2022; Evans et al., 2017). Therefore, there is mounting evidence that lakes function as "biogeochemical reactors", receiving terrestrial C and continuously cycling the bulk of aquatic C (Pi et al., 2022; Rodríguez-Cardona et al., 2023). Yet to date, the mechanisms driving lake C cycling are poorly understood, particularly regarding the underlying factors that constrain C emission (Chen et al., 2022; Mendonça et al., 2017). It is estimated that inland lakes, despite covering only ~3% of the land surface, contribute to 38% of aquatic C outgassing (Tranvik et al., 2009). Although the drivers of these emissions are regionally investigated (Maberly et al., 2013; Mu et al., 2023; Serikova et al., 2019), a fundamental factor governing C fixation, mineralization, and subsequent uptake or release remains elusive. Deciphering the cycling of dissolved C offers a promising avenue to address this knowledge gap, as it mediates C turnover between organic and inorganic forms and accounts for ~90% of the global C flux from terrestrial to aquatic ecosystems (Drake et al., 2020), making it essential for understanding aquatic C budget (Raymond and Hamilton, 2018; Song et al., 2018).

Evidence suggests that seasonal wetness and drought control the dynamics of dissolved inorganic C (DIC) concentrations and species (Rehn et al., 2023; Tye et al., 2022). These events also alter water-land connectivity and thus the export of dissolved organic C (DOC) to inland waters (Li et al., 2022a; Wang et al., 2024; Yuan et al.,

2024). Subsequently, aquatic photosynthesis utilizes DIC, while heterotrophic respiration fuelled by DOC~~heterotrophic respiration of DOC~~ generates CO_2 (Guo et al., 2023; Leles and Levine, 2023). Consequently, dissolved C turnover and CO_2 emissions are anticipated to be highly interconnected through hydrological and biological mechanisms (Hu et al., 2022; Kellerman et al., 2014; Monteith et al., 2023). For example, experimental data suggest that droughts can stimulate dissolved C cycling by transiently accelerating primary production and, more persistently, DOC respiration (Harjung et al., 2019).

These pervasive turnover and emission of aquatic C, in particular, can be substantial in karst waters. The prevailing view suggests the regional specificity of karst regions, specifically with respect to ecological fragility and the significant role in carbonate C sink (Chen et al., 2023; D'Ettorre et al., 2024). Yet, recent reports also highlight significant dissolved C cycling and CO_2 sequestration in karst aquatic ecosystems, attributed to the "biological C pump" effect (He et al., 2024; Sun et al., 2022; Zhang et al., 2024). Carbonate weathering can couple with photosynthetic uptake of DIC, resulting in self-amplifying CO_2 sink during karst water cycle (Liu et al., 2018; Wang et al., 2022). Nevertheless, primary production may trigger DOC catabolism and rapid cycle of active C (Ni et al., 2023; Ni et al., 2022). These critical processes are tightly linked to~~are associated with~~ microbially mediated C fixation and mineralization~~aquatic biology~~, but little is known about how lake microorganisms drive dissolved C turnover and ultimately modulate CO_2 emissions in karst lakes.

Theoretically, aquatic microbial community in karst lakes is expected to regulate DIC-DOC transformation, whereby microbially mediated C fixation and mineralization shift the balance between CO_2 production and consumption ~~Theoretically, microbiome is anticipated to govern internal cycling between DIC and DOC, and this process, in turn, may affect specific CO_2 pathways~~ (Li et al., 2022b; Shangguan et al., 2024). Prior studies found significant DIC uptake by C-fixing microorganisms (Li et al., 2024) and recalcitrant DOC sequestration *via* heterotrophic bacteria in karst aquatic systems (He et al., 2022b; Xu et al., 2023), which potentially regulate CO_2 fixation and outgassing in response to ~~specific~~ temporal pathways of C metabolism. Because hydrologic wet-dry shifts can restructure aquatic habitats and substrate availability for microorganisms, we thus hypothesized that wet and drought conditions will shift microbial metabolic strategies, thereby modulating dissolved C turnover and CO_2 dynamics in karst lakes.~~Therefore, we hypothesized that microorganisms will interact with dissolved C to establish distinctive CO_2 drivers in karst lakes.~~ To test this hypothesis, we conducted a two-year investigation, capturing an extreme drought event and its following rainfalls, with the aims of revealing: 1) temporal interactions of aquatic microbiome with dissolved C dynamics; 2) specific pathways governing karst lake CO_2 flux; and 3) microbially-driven dissolved C turnover and the resulting CO_2 emission or sequestration. Achieving these aims is expected to uncover the underlying mechanisms of C source-sink transformation in karst water environments, ultimately supporting efforts toward C neutrality.

Formatted: Subscript

Formatted: Subscript

2. Materials and methods

2.1. Study area

Observations were performed in the karst lakes Hongfeng (HFH), Laoma (LMH) and Baihua (BBH), located between 25º57′ to 26º42′N in latitude and 105º58′ to 106º34′E in longitude (Fig. 1). The catchment geology is predominantly karst lithology i.e., dolomite and limestone. Lake HFH and BHH, two of the largest artificial lakes in Guizhou Province, cover surface areas of 57.2 and 14.5 km^2, with water volumes of 6.01×10^8 and 1.91×10^8 m^3, respectively. As a segment of the Maotiao River, the LMH is supplied by several tributaries that connect Lake HFH to BHH. These karst waters are situated in a subtropical monsoon climate zone, with annual temperatures ranging from -7.8°C to 37.5°C. The wet season lasts from May to October, delivering an average annual precipitation of 1130 mm. Specifically, an extreme drought event occurred in 2022–2023, with monthly rainfall <10 mm during the drought (early winter), >100 mm during the initial-wet (early summer), and 50–100 mm during the post-wet (autumn) periods. These lakes, which serve as drinking water sources, are impacted by ~~acting as drinking water sources, are disrupted by~~ agriculture and domestic sewage.

2.2. Fieldwork and laboratory analysis

During May to November from 2022 to 2023, our sampling captured an extreme drought event, allowing us to clearly identify the specific temporal scales during the

drought, initial-wet and post-wet periods. Spatially, fieldworks were designed to incorporate full spectrum of the karst lakes from 32 sampling locations (Fig. 1~~a~~). Therefore, a total of 96 water samples were collected from our investigations. In detail~~s~~, we collected surface waters at a depth of ~10 cm and filtered them within 6 hours. Filtrates were stored in 1000-mL high-density polyethylene (HDPE) containers designed to eliminate headspace and air bubbles. Water samples were filtered using glass microfiber filters (Whatman, GF/F 47 mm, 0.7-μm) for dissolved C measurement, and polycarbonate membrane filters (Millipore, ~~GF/F~~ 47 mm, 0.22-μm) for microbial determination. Samples were refrigerated at 4°C during transport and stored at -70°C for microbiological analysis.

Water temperature and pH were *in-situ* determined with a portable pH meter (PHB-4, Shanghai). Wind velocity was measured using a Testo 410-1 anemometer (Testo, Germany). Total alkalinity was titrated with Alkalinity Test MColortestTM (Merck, Germany). DOC concentration was detected using varioTOC cube/select (Elementar, Germany). Chromophoric DOC was determined using a double-beam scanning spectrophotometer (UV-5500PC, Shanghai) with UV–visible absorption spectra ranging from 200 to 700 nm (1-nm interval). Fluorescence DOC was analysed using a RF-6000 Spectrophotometer (Shimadzu, Japan), with excitation and emission wavelengths of 200–450 (5-nm interval) nm and 250–600 nm (1-nm interval), respectively. Molecular DOC was characterized using Fourier transform ion cyclotron resonance mass spectrometry (FT-ICR MS). We combined equal volumes of water

samples from each lake site, leaving us three composite samples for FT-ICR MS analysis. Details on sample pretreatment (solid-phase extraction, SPE) for FT-ICR MS are available in Supplementary Text S1.

Genomic DNA in sampling waters was extracted using E.Z.N.A. Water DNA Kit (OMEGA, USA) according to the manufacturers' instructions, and assessed~~detected with~~ by 1% agarose gel electrophoresis. ~~It employed u~~Universal primers 341F (5'-CCTAYGGGRBGCASCAG-3') and 806R (5'-GGACTACNNGGGTATCTAAT-3') were used to amplify the~~for amplifying the~~ V3–V4 hypervariable region of the 16S rRNA, with a GeneAmp PCR System 9700 (ABI GeneAmp, USA). The PCR products were extracted by 2% agarose gel electrophoresis, and recovered from AXYPREP DNA Gel Recovery Kit (Axygen Biosciences, USA) with Tris-HCl for elution. Purified amplicons were pooled in equimolar and sequenced using paired-end on an Illumina MiSeq PE300 (Illumina, USA) following standard protocols.

2.3. Data processing and calculation

In this study, we employed a carbonate equilibrium~~equilibria~~-based method for estimating aqueous DIC, using combinations of water chemistry parameters (pH, water temperature and total alkalinity) through CO_2SYS program (Xu et al., 2017). This program outputs concentrations of DIC species i.e., total DIC, HCO_3^-, CO_3^{2-} and dissolved CO_2, as well as aqueous partial pressure of CO_2 (pCO_2), a crucial indication for potential CO_2 emissions from aquatic environments. The following thin boundary

188 layer model was used to calculate areal CO_2 flux (mmol m^{-2} d^{-1}) from the karst waters.

189

190 $$Areal\ CO_2\ flux = (pCO_{2water} - pCO_{2ir}) \times k \times K_h \quad (1)$$

191

192 This model proposes that the difference between aqueous (pCO_{2water}, μatm) and
193 atmospheric pCO_2 (pCO_{2air}, μatm) can characterize the impetus and direction for CO_2
194 transfer. Temporal shifts in *in-situ* atmospheric CO_2 levels (dimensionally convertible
195 to pCO_{2air}) are available in Fig. S1. By contrast, gas transfer velocity (k, m d^{-1}) can
196 constrain the velocity of water-air CO_2 exchange, which is calibrated from normalized
197 gas transfer velocity (k_{600}, cm h^{-1}) using water temperature and Schmidt number.
198 Specifically, k or k_{600} serves as a function of water turbulence, empirically modelled
199 by wind velocity in lakes and lentic rivers. Henry's constant (K_h, mmol m^{-3} μatm^{-1})
200 calibrated from *in-situ* temperature and pressure, characterizes CO_2 equilibrium at
201 water-air interfaces. Details for chemical calculations of DIC species and thin
202 boundary layer model are provided in~~see~~ Supplementary Text S2.

203

204 We analysed UV–visible and fluorescent spectroscopy to~~for~~ understand~~ing~~ DOC
205 component, origin and fate. Specifically, DOC-normalized absorption coefficient
206 $SUVA_{254}$ (L mg^{-1} m^{-1}), an indicator of DOC aromaticity, was computed as the
207 absorption coefficient (a_{254}, m^{-1}) divided by DOC concentration (mg L^{-1}). Spectral
208 slope $S_{275\text{-}295}$, a proxy for DOC relative molecular weight, was calculated by
209 nonlinearly fitting an exponential function to the absorption spectrum from 275 to 295

nm. Fluorescence index (FI) increases with intensified biological activity, and indicates allochthonous (< 1.4) and autochthonous (> 1.9) inputs for aquatic DOC, which was calculated as the ratio of emission intensity at 470 nm to 520 nm with an excitation of 370 nm. Biological index (BIX), a proxy for freshness of biologically produced DOC, was calculated as the ratio of emission intensity at 380 nm to 430 nm, using an excitation of 310 nm. Humification index (HIX), characterizing to DOC humification and biodegradability, was expressed as the ratio of total emission intensities at 435–480 nm divided by 300–345 nm, at an excitation of 254 nm. Parallel factor analysis (PARAFAC) was used to identify primary DOC components by separating excitation-emission matrices into independent fluorophores. The PARAFAC modelling employed residual and split-half analyses for component selection and correspondence validation.

FT-ICR MS analysis was conducted to examine dissolved organic matter (DOM, represents the specific material form of the general DOC) composition using a molecular formula calculator based on criteria with elemental combinations of $C_{0-\infty}H_{0-\infty}O_{0-\infty}N_{0-1}S_{0-1}$. Peaks were detected within S/N >4 and a mass accuracy of ≤ ±1 ppm. Van Krevelen diagrams plotting H/C against O/C were employed to visualize FT-ICR MS data. Seven DOM compositions were extracted based on the elemental ratios of H/C and O/C (Ni et al., 2024), involving carbohydrates, amino-sugars, saturated compounds, tannins, lignin, unsaturated hydrocarbons and condensed aromatic structures. The elements (C, H, O, N, P and S), and formulas (CHO, CHOS, CHON,

CHOP, CHONS, CHONP, CHOSP and CHONSP) were identified based on molecular exact mass and matched against a molecular formula database~~formulas database~~ (Yan et al., 2024). The modified aromaticity index (AI-mod) and nominal oxidation state of carbon (NOSC) were calculated as follows:

$$AI\_mod = \frac{1 + \mathrm{C} - \frac{1}{2}O - S - \frac{1}{2}(N + H)}{\mathrm{C} - \frac{1}{2}O - N - S} \quad (2)$$

$$NOSC = \frac{4\mathrm{C} + \mathrm{H} - 3\mathrm{N} - 2\mathrm{O} - 2\mathrm{S}}{\mathrm{C}} \quad (3)$$

Alpha diversity, calculated using Mothur (https://mothur.org/wiki/calculators/), was used to assess microbial community using~~through~~ the indices Coverage (community coverage), Chao (community richness) and Shannon (community diversity). We analysed microbial community and its relative abundance, ranking the top 20 microorganisms at genus level. Using Tax4Fun, we converted 16S into prokaryotic classification profiles in the KEGG database, enabling KEGG functional annotation for 16S RNA gene sequences. It provides insights into potential microbial functions based on their composition and abundance in aquatic environments, and specifically presents information on KEGG Orthology in this study.

2.4. Data q~~Q~~uality ~~control~~

Water collection and analysis followed the standard procedures, as proposed by the American Public Health Association (1985).~~–~~ However, we acknowledge that (1)

temporally, discrete surface sampling may omit short-lived C dynamics driven by diel variability and episodic event (e.g., flooding and thermal fluctuations); and (2) spatially, surface measurements at limited stations may not fully represent horizontal heterogeneity (e.g., differences in macrophytes and local human activities). Therefore, we interpret our results as evidence for surface water patterns during the observed period and avoid extrapolating the frequency and magnitude of CO_2 pulses without higher-frequency and multi-site observations. The pH probe was calibrated with 6.86 and 9.18 pH standard solution at 25°C, ensuring ±0.01 pH unit accuracy. Water temperature and wind velocity were accurate to ±0.5°C and ± (0.2 m/s + 2% of measurements), respectively. Alkalinity Test MColortestTM measured total alkalinity with < 3% uncertainty.

Lake DIC species calculated from water chemistry may be overestimated due to non-carbonate alkalinity (Liu et al., 2020). We specifically assessed that non-carbonate alkalinity from nitrogen, phosphorus and organic C can result in a maximum 29.5% overestimation of DIC species. Consequently, we corrected this overestimation by using measured DIC concentrations (Fig. S2), which converted systematic errors into instrument errors (< 2%) for all DIC datasets. UV measurements were 10% replicated, suggesting an uncertainty of < 2 %. The inner filter effect of fluorescence data can be neglected since absorbances at 254 nm were all below 0.3 (Ohno, 2002). Excitation-emission matrices were corrected for Raman and Rayleigh scatterings through interpolation, and fluorescence intensity (A.U.) was

Formatted: Subscript

Formatted: English (United States)

Formatted: Indent: First line: 2 ch

normalized to Raman Unit (R.U.) *via* water Raman peak areas (Ni et al., 2024). FT-ICR MS and microbial analysis were conducted by China National Analytical Centre (Guangzhou, China) and Majorbio Bio-Pharm Technology Co. Ltd. (Shanghai, China), respectively.

2.5. Statistical analysis

Normality and homogeneity of variance were assessed using Kolmogorov-Smirnov test and Levene's test, respectively. Variables were log-transformed as needed to ensure normality assumptions. One-way analysis of variance (ANOVA) with Tukey HSD post hoc was employed to evaluate statistical differences across DIC species, DOC compositions and microbial variables. Correlation analysis was used to assess possible associations within or between dissolved C, CO_2 flux and microbial variables. We introduced a structural equation model (SEM) to examine how aquatic microorganisms interact with dissolved C and ultimately influence CO_2 flux through both direct and indirect pathways. We initially excluded the variables with nonlinear relationships (e.g., alpha diversity and Tax4Fun) to derive comparable standardized path coefficients. We further established and specified 6 latent variables according to the loadings of their associated observed variables (see Supplementary Text S3). In the SEM, we hypothesized that 1) photosynthetic and heterotrophic microbes will preferentially associate with DIC for anabolism and DOC for catabolism, respectively; and 2) dissolved C dynamics and CO_2 flux are intertwined due to carbonate chemistry, biogenic, and terrestrial regulations. The SEM with partial least

squares path modelling was performed using the plspm package in R (Version 4.1.3). Statistical analyses and figure preparation~~figures preparing~~ were conducted using and OriginPro 2024 and MATLAB 2018.

3. Results

3.1. DIC species and CO_2 emissions

The significant carbonate kinetics in karst waters present an opportunity to understand the dynamics of aqueous DIC species. This study captured strong seasonality in water chemistry (Table 1), particularly with lower pH and water temperature during the extreme-drought period ($p < 0.001$ by ANOVA). *In-situ* measured total alkalinity (range: 2178.7–6210.8 μeq L^{-1}), along with DIC (range: 1538.7–6206.0 μmol L^{-1}) and HCO_3^- (range: 918.4–5970.6 μmol L^{-1}), had no temporal variations across the periods ($p > 0.05$). Extreme drought caused lower aqueous CO_3^{2-} but higher dissolved CO_2 levels in comparison to wet conditions ($p < 0.001$, Fig. S3). It should be noted that we corrected concentrations of DIC species by eliminating systematic errors from non-carbonate alkalinity, reducing average uncertainties of 6.8% for DIC, 7.0% for HCO_3^-, and 38.7% for dissolved CO_2 (Fig. S2).

To estimate potential CO_2 emissions from the study lakes, we calculated aqueous pCO_2, k and areal CO_2 flux (Fig. 2~~1~~). These lakes had a broad range of aqueous pCO_2 levels, spanning from 20 to 13479 μatm across sampling locations (Fig. ~~1b~~2a). We found that extreme drought (4437 ± 3468 μatm) unexpectedly caused a ~five-fold

increase in mean pCO_2 relative to initial- (804 ± 1080 µatm) and post-wet periods (928 ± 1728 µatm, $p < 0.001$), which can escalate to ~ten-fold when considering median pCO_2 (Fig. ~~1b~~2a). Indeed, our dataset reveals that 61% of samples were oversaturated with CO_2 relative to atmospheric equilibrium (Fig. S1), attributable to high pCO_2 levels during extreme droughts. Gas transfer velocity k showed no significant temporal shifts ($p > 0.05$), ranging from 0.37–2.28 m d^{-1} with a mean of 0.62 ± 0.26 m d^{-1} (Fig. ~~1c~~2b). This is slightly lower than previously reported global average of 0.74 m d^{-1} from a similar empirical model based on wind speed (Raymond et al., 2013). We estimated areal CO_2 flux to be 42 ± 79 mmol m^{-2} d^{-1} (range: -24–459 mmol m^{-2} d^{-1}) from the karst lakes. However, it is also noted that the bulk of samples during wet periods were undersaturated (Fig. ~~1d~~2c). We show that the extreme drought increased areal CO_2 efflux sharply (111 ± 104 mmol m^{-2} d^{-1}), relative to initial- (6 ± 22 mmol m^{-2} d^{-1}) and post-wet periods (10 ± 26 mmol m^{-2} d^{-1}) in our observed episode ($p < 0.001$). Our findings, therefore, may partially deviate from the previous understanding of aquatic karst carbon sinks (An et al., 2015; Binet et al., 2020; Liu et al., 2010), indicating that karst lakes could be a significant source of CO_2 driven by extreme drought events.

3.2. DOC composition, origin and fate

We used spectroscopic and molecular methods to assess DOC composition, origin and fate (Fig. ~~2~~ 3 and ~~3~~4). Aqueous DOC concentrations had a ~30-fold variation (range: 0.76–22.1 mg L^{-1}) across the samplings (Fig. ~~2a~~3a). Extreme drought apparently

elevated DOC concentrations to an average of 12.4 ± 3.7 mg L^{-1}, relative to initial- (5.4 ± 2.3 mg L^{-1}) and post-wet periods (5.7 ± 1.6 mg L^{-1}) ($p < 0.001$). DOC aromaticity descended significantly across the periods, with initial-wet > post-wet > extreme drought ($p < 0.01$), as suggested by $SUVA_{254}$. By contrast, relative molecular weight of DOC, indicated by $S_{275\text{-}295}$, was higher during extreme-drought period than wet periods ($p < 0.05$). We were able to identify DOC fluorescent component through PARAFAC, demonstrating two distinct humic-like (both classified as C1) and one tryptophan-like DOC (C2) across the periods (Fig. ~~2b~~3b). The temporal abundances differed significantly ($p < 0.001$), with %C1 > %C2 during the extreme drought yet %C1 < %C2 during wet conditions (Fig. S4). These karst waters received both allochthonous and autochthonous inputs, with 80% of samples falling within the FI range of 1.4–1.9 (Fig. ~~2c~~3c). As suggested by BIX, we found biologically produced young DOC was more abundant during initial-wet than extreme-drought period ($p < 0.05$). However, DOC humification proxied by HIX was notably greater during the extreme drought than that in the wet conditions ($p < 0.01$).

We identified~~It captured the~~ molecular formulas for a total of 8060, 8636 and 8403 FT-ICR-MS compounds in lake LMH, HFH and BHH, respectively (Fig. ~~3~~4). The molecular formulas were classified into distinct categories based on H/C and O/C distributions, as well as exact mass in van Krevelen Diagram (Fig. ~~3a~~4a). The study lakes showed a similar range of DOM exact mass, varying from 114.031694 to 1121.181055 Da. We suggest that these lakes were governed by low-molecular-weight

DOM, with 80%, 74%, and 77% of the detected molecules for LMH, HFH, and BHH having an exact mass < 500 Da, respectively. The summed intensity was highly variable for each DOM molecular category, notably with lignin compounds (or carboxy-rich acyclic molecules) comprising 83%–84%, followed by saturated compounds at 11%–13% across lakes. Amino-sugars also represented a notable 1.8%–2.3%, while carbohydrate, tannins, unsaturated hydrocarbons and condensed aromatic structures each occupied ≤ 1% across all molecular categories. These DOM molecules were largely comprised of atomic groups CHO (44.8%–49.2%), CHOS (17.2%–25.5%), CHON (19.2%–26.6%) and CHONS (5.6%–6.3%) (Fig. ~~3b~~4b). Each karst lake shared a comparable average AI_{mod} across FT-ICR-MS compounds ($p > 0.05$), while NOSC was higher in lake BHH (-0.29 ± 0.48) than that in ~~LHM~~ LMH (-0.32 ± 0.48) ($p < 0.01$, Fig. ~~3c~~4c).

3.3. Aquatic microbiome in the karst lakes

To evaluate microbial processes in the karst lakes, we examined temporal variability of microbiome from 89 samples (Fig. ~~4~~5). For the microbial diversity, a total of 121–351 ASV (14382 sequences), 236–479 ASV (40251 sequences) and 143-445 ASV (42507 sequences) were assigned during the extreme-drought, initial-wet and post-wet periods, respectively (Fig. S5). Rainfall increased microbial richness and diversity in the aquatic environment (Fig. ~~4a~~5a), as indicated by Chao (initial wet > post wet > extreme drought, $p < 0.05$) and Shannon (initial wet > post wet and extreme drought, $p < 0.05$). However, microbial coverage was higher in the extreme-drought period (p

< 0.01). The top 3 microorganisms were *Acinetobacter*, *CL500-29_marine_group* and *Cyanobium_PCC-6307* at genus level, with the average relative abundances of 11.6% ± 10.3%, 10.3% ± 5.58% and 5.68% ± 3.91%, respectively (Fig. ~~4b~~5b). *Acinetobacter* and *CL500-29_marine_group*, important for C catabolism, had increased relative abundance during the extreme drought. By contrast, photosynthetic microorganisms *Cyanobium_PCC-6307* and *g_norank_f__norank_o__Chloroplast* were more abundant during the initial-wet period (Fig. ~~4b~~5b). Therefore, we found that amino acid catabolism was significant under extreme droughts, while carbohydrate anabolism was predominant under wet conditions (Fig. ~~4c~~5c, $p < 0.001$).

4. Discussion

4.1. Temporal interactions of aquatic microbiome with dissolved C dynamics

Karst aquatic ecosystems, with rapid kinetics of carbonate chemistry and biological metabolism involved, may develop associated strategies for dissolved C turnover (He et al., 2024; Ni et al., 2023; Xi et al., 2024). Here, our results show the consistent shifts of dissolved C with aquatic microbiome in karst lakes. Extreme droughts, for instance, set the stage for substantial proliferation of heterotrophic microbes (Fig. ~~4b~~5b) and thus microbial degradation of enriched DOC (Fig. ~~2a~~3a). As labile DOC is exhausted, these microbes are compelled to metabolize typically more refractory DOC. This aligns with recent observations in karst and thermokarst lakes (Hu et al., 2023; Ni et al., 2022), as also evidenced by the parallel increase in CO_2 levels (Fig. ~~1b~~2) and decrease in DOC aromaticity (Fig. ~~2~~3a), suggesting that in-lake aromatic

compounds are partially labile during extreme droughts. By analysing DOC molecular composition, we specifically found that N-containing, rather than S-containing aromatics are more bioavailable for heterotrophic microorganisms (Fig. S6 and Supplement table S1).

Rainfall accelerates atmospheric CO_2 uptake and CO_3^{2-} generation in karst aquatic environments (Zhao et al., 2024), which, combined with photosynthetic uptake of DIC, provides conditions for the enhancement of photosynthetic microorganisms (Fig. ~~4b~~5b). This explains the consistently low CO_2 levels during wet periods (Fig. ~~1b~~2a), aside from the known dilution effect (Ni et al., 2019). Here, we suggest that initial rainfall following extreme droughts substantially boosts microbial richness and diversity (Fig. ~~4a~~5a), possibly due to amplified terrestrial inputs and rejuvenated aquatic biology (Fig. S7). Moreover, we were able to examine the associations between DOC molecular compositions and microorganisms, revealing that photosynthetic microorganisms generate substantial quantities of biodegradable DOC e.g., carbohydrate and lipid-like compounds (Fig. S6 and Supplement table S1). Therefore, our results indicate season-specific microbial strategies for dissolved C metabolism in karst lakes.

4.2. Specific pathways governing karst lake CO_2 flux

Microbiome-driven dissolved C turnover can further alter CO_2 dynamics, especially in lakes with long-term hydraulic retention and active biological processes (Lindström

and Bergström, 2004). Our results show that the photosynthesis-driven associations between microbiome, dissolved C, and CO_2 flux emerged substantially during initial-wet periods (Fig. S8). Studies previously predicted self-amplifying photosynthesis driven by carbonate dissolution in karst waters (He et al., 2022a; Liu et al., 2010). Here, we present direct evidence that photosynthetic microorganisms dominate the microbial communities during the initial-wet period (Fig. ~~4b~~5b). Extreme drought, however, decouples the linkages between dissolved C and CO_2 flux from photosynthetic microorganisms. Respiration of DOC e.g., tryptophan-like component in turn fuels lake CO_2 during the extreme-drought period (Fig. S8). Our data allow us to extrapolate that amino acids, aliphatic compounds and small molecular organic acids serve as primary substrates driving CO_2 production and emissions in these lakes (Fig. S9 and Supplement table S1).

Using SEM, we clearly demonstrate the specific pathways governing lake CO_2 transfer across the periods (Fig. ~~5~~6). Our observations reinforce that extreme droughts stimulate microbial metabolism of aromatic DOC and contribute to CO_2 outgassing from the study lakes (Fig. ~~5a~~6a). Nevertheless, an alternative C metabolism pathway emerged~~it emerged an alternative C metabolism pathway~~ during the initial-wet period (Fig. ~~5a~~6a): photosynthetic microorganisms constrain DIC species and subsequent CO_2 flux in lakes. This photosynthetic pathway persisted during the post-wet period, yet we found a specific pathway involving aquatic microbes that promotes a decrease in molecular size and subsequent increases in humic-like abundance (Fig. ~~5a~~6a). This

observation aligns with a previous study in karst aquatic ecosystems (Xia et al., 2022), suggesting that intense photosynthesis produces labile compounds and subsequently activates the catabolism of DOC pool, ultimately resulting in the selective accumulation of recalcitrant compounds. These findings, complement prior evidence from biodegradation assays (Ni et al., 2022), providing a new insight into photosynthetic products triggering significant microbial activities and dissolved C turnover in karst lakes.

4.3. Implications for biologically driven C cycling in karst waters

Karst aquatic ecosystems typically represent strong interactions between microbial metabolism and dissolved C turnover, driven by the known "biological C pump" (Yi et al., 2021; Zhang et al., 2024). While the specific C sink from this mechanism is well-documented (Cao et al., 2018; Chen et al., 2023; Sun et al., 2021), the causes of periodic C evasion from karst waters are still questionable. In this study, we propose that the observed ~~extreme~~ extreme-drought event~~s~~ yielded large CO_2 emissions from the karst lakes, increasing >10 times on average relative to wet conditions (Fig. ~~1d~~2c). Droughts apparently accelerate DOC-fuelled heterotrophic respiration ~~heterotrophic respiration of DOC~~, acting as a primary mechanism fuelling in-lake CO_2. Drought-enriched heterotrophic microorganisms extensively deplete labile DOC, and even resort to metabolizing previously recognized recalcitrant compounds. Aromatic DOC, for instance, characterized by microbial resistance, has recently been reported to be activated through photochemistry (Hu et al., 2023). Here, our results demonstrate a

clear mechanism by which microbial degradation of N-containing aromatic compounds contributes to C metabolism (Fig. S6), indicating that extreme droughts suppress biological C sink in karst lakes.

Wet conditions in karst lakes, in contrast, show a distinct pathway governed by aquatic photosynthesis (Fig. ~~5b~~6b), aligning with the prior theory regarding karst biological C sink (Liu et al., 2018). This stimulates a substantial uptake of CO_2 and thus limit lake C emission. Our observations provide direct evidence that photosynthetic microorganisms produce carbohydrates and promote the formation of lipid-like (Fig. S6) as well as other low-molecular-weight compounds (Fig. S8). These labile DOC quickly engage in subsequent biological processes, accelerating the proliferation of heterotrophic microorganisms. Our efforts to upscale this mechanism demonstrate a clear causality: 1) catabolism of photosynthetically derived labile DOC stimulates heterotrophic microorganism growth; 2) recalcitrant DOC accumulates relatively as heterotrophic respiration increases, even though aromatic compounds are partially utilized; and 3) a priming effect is triggered, promoting both labile DOC mineralization to CO_2 and the sequestration of recalcitrant DOC. These findings highlight that biologically driven organic C turnover critically determine the CO_2 uptake or release in karst aquatic ecosystems.

Overall, consistent with our hypothesis~~as we initially hypothesized~~, wet-dry seasonality shifted microbial metabolic strategies and altered temporally structured

turnover between DIC and DOC, thereby regulating CO_2 uptake and evasion in the karst lakes. ~~aquatic microbiome interacts with dissolved C dynamics, establishing the distinctive CO_2 driving mechanisms that particularly fluctuate with biochemical timing in karst lakes.~~ It is anticipated that pulses of CO_2 emissions will occur after wet conditions end, particularly under drought conditions, as a result of rapid decay of photosynthetically derived organic C. Therefore, managing C sink in karst aquatic systems depends heavily on mitigating the sudden bursts of DOC respiration, especially the dramatic increased CO_2 release during extreme droughts. Our results indicate that wet conditions significantly enhance biological strategies for CO_2 uptake in karst aquatic ecosystems, highlighting the crucial role of mitigating climate change-induced droughts in strengthening karst C sink.

4. Conclusion

Karst lakes represent distinctive microbial pathways for dissolved C metabolism and subsequent CO_2 sequestration or emission. Here, we specifically reveal the temporal dynamics of CO_2 fluxes driven by periodic interactions between aquatic microbiome and dissolved C turnover in the study karst lakes. We show that extreme droughts accelerate the proliferation of heterotrophic microbes and thus rapid respiration of DOC, resulting in a sharp increase in CO_2 emissions. By contrast, wet conditions stimulate aquatic photosynthesis, which consumes DIC and sequesters CO_2 within the lakes. We highlight that exhausted DOC compels heterotrophic microorganisms to metabolize refractory N-containing aromatic compounds, while photosynthetic

microorganisms promote the formation of labile DOC compounds. These specific microbial strategies indicate that in our observed episode, pulsed CO_2 outgassing from karst lakes may occurs after periods of high photosynthetic activity, with the magnitude being significantly amplified during extreme droughts. Therefore, we propose that managing periodic CO_2 outgassing, particularly during droughts, is essential for developing C neutrality in karst waters.

Code/Data availability

The full dataset used for the evaluation of this study is publicly available at https://figshare.com/s/7475752c5f7b19718199.

Declaration of Competing Interest

All authors agree to this submission and declare that there are no conflicts of interest regarding the publication of this article

Author contributions

The project was conceived by M.N. and Z.K. M.N. directed and managed the study, as well as prepared the first draft of the manuscript. Z.K. collected and analysed samples, contributed to data interpretation and paper writing. G.Z. specified the experimental conditions and measured CO_2 data. W.L. specified the experimental conditions and contributed to CO_2 data analysis and interpretation. J.P. conceptualized dissolved carbon turnover in this study, and contributed to data interpretation and

paper writing. X.L. performed the structural equation model and generated its original figure. J.C. and J.Z. and X.W. provided comments on the manuscript. All authors reviewed and contributed to the final manuscript.

Acknowledgments

This study was financially supported by the National Natural Science Foundation of China (NSFC grant no. U2244216, 42167050, 42407094), National Special Support Plan for High-Level Talent to Junbing Pu (Young Talent Plan, 2022), Natural Science Foundation of Chongqing, China (CSTB2022NSCQ-LZX0022, 2024NSCQ-MSX3061), Guizhou Provincial Platform and Talent Program (YQK [2023]017), Guizhou Provincial Science and Technology Projects (ZK[2024]061), Science and Technology Plan for High-Level Young Talent of Guizhou Education Department ([2024]325) and the Second Tibetan Plateau Scientific Expedition and Research Program (Sub-item: 2019QZKK0601-3). Special thanks are given to the editor, and two anonymous referees for their constructive comments and suggestions.

References

An, Y., Hou, Y., Wu, Q., Qing, L., and Li, L.: Chemical weathering and CO_2 consumption of a high-erosion-rate karstic river: a case study of the Sanchahe River, southwest China, Chinese Journal of Geochemistry, 34, 601-609, 2015.

Binet, S., Probst, J. L., Batiot, C., Seidel, J. L., Emblanch, C., Peyraube, N., Charlier, J. B., Bakalowicz, M., and Probst, A.: Global warming and acid atmospheric deposition impacts on carbonate dissolution and CO_2 fluxes in French karst hydrosystems: Evidence from hydrochemical monitoring in recent decades, Geochimica et Cosmochimica Acta, 270, 184-200, 2020.

Bogard, M. J., Kuhn, C. D., Johnston, S. E., Striegl, R. G., Holtgrieve, G. W., Dornblaser, M. M., Spencer, R. G. M., Wickland, K. P., and Butman, D. E.: Negligible cycling of terrestrial carbon in many lakes of the arid circumpolar landscape, Nature Geoscience, 12, 180-185, 2019.

Borges, A. V., Deirmendjian, L., Bouillon, S., Okello, W., Lambert, T., Roland, F. A. E., Razanamahandry, V. F., Voarintsoa, N. R. G., Darchambeau, F., Kimirei, I. A., Descy, J.-P., Allen, G. H., and Morana, C.: Greenhouse gas emissions from African lakes are no longer a blind spot, Science Advances, 8, eabi8716, 2022.

Cao, J.-h., Wu, X., Huang, F., Hu, B., Groves, C., Yang, H., and Zhang, C.-l.: Global significance of the carbon cycle in the karst dynamic system: evidence from geological and ecological processes, China Geology, 1, 17-27, 2018.

Chen, H., Ju, P., Zhu, Q., Xu, X., Wu, N., Gao, Y., Feng, X., Tian, J., Niu, S., Zhang, Y., Peng, C., and Wang, Y.: Carbon and nitrogen cycling on the Qinghai–Tibetan Plateau, Nature Reviews Earth & Environment, 3, 701-716, 2022.

Chen, L., Tan, L., Zhao, M., Sinha, A., Wang, T., and Gao, Y.: Karst carbon sink processes and effects: A review, Quaternary International, 652, 63-73, 2023.

D'Ettorre, U. S., Liso, I. S., and Parise, M.: Desertification in karst areas: A review, Earth-Science Reviews, 253, 104786, 2024.

Drake, T. W., Podgorski, D. C., Dinga, B., Chanton, J. P., Six, J., and Spencer, R. G. M.: Land-use controls on carbon biogeochemistry in lowland streams of the Congo Basin, Global Change Biol, 26, 1374-1389, 2020.

Evans, C. D., Futter, M. N., Moldan, F., Valinia, S., Frogbrook, Z., and Kothawala, D. N.: Variability in organic carbon reactivity across lake residence time and trophic gradients, Nature Geoscience, 10, 832-835, 2017.

Guo, Y., Gu, S., Wu, K., Tanentzap, A. J., Yu, J., Liu, X., Li, Q., He, P., Qiu, D., Deng, Y., Wang, P., Wu, Z., and Zhou, Q.: Temperature-mediated microbial carbon utilization in China's lakes, Global Change Biol, 29, 5044-5061, 2023.

Harjung, A., Ejarque, E., Battin, T., Butturini, A., Sabater, F., Stadler, M., and Schelker, J.: Experimental evidence reveals impact of drought periods on dissolved organic matter quality and ecosystem metabolism in subalpine streams, Limnology and Oceanography, 64, 46-60, 2019.

He, H., Liu, Z., Li, D., Liu, X., Han, Y., Sun, H., Zhao, M., Shao, M., Shi, L., Hao, P., and Lai, C.: Effects of carbon limitation and carbon fertilization on karst lake-reservoir productivity, Water Research, 261, 122036, 2024.

He, H., Wang, Y., Liu, Z., Bao, Q., Wei, Y., Chen, C., and Sun, H.: Lake metabolic processes and

their effects on the carbonate weathering CO_2 sink: Insights from diel variations in the hydrochemistry of a typical karst lake in SW China, Water Research, 222, 118907, 2022a.
He, Q., Xiao, Q., Fan, J., Zhao, H., Cao, M., Zhang, C., and Jiang, Y.: The impact of heterotrophic bacteria on recalcitrant dissolved organic carbon formation in a typical karstic river, Sci Total Environ, 815, 152576, 2022b.
Hu, A., Choi, M., Tanentzap, A. J., Liu, J., Jang, K.-S., Lennon, J. T., Liu, Y., Soininen, J., Lu, X., Zhang, Y., Shen, J., and Wang, J.: Ecological networks of dissolved organic matter and microorganisms under global change, Nat Commun, 13, 3600, 2022.
Hu, J., Kang, L., Li, Z., Feng, X., Liang, C., Wu, Z., Zhou, W., Liu, X., Yang, Y., and Chen, L.: Photo-produced aromatic compounds stimulate microbial degradation of dissolved organic carbon in thermokarst lakes, Nat Commun, 14, 3681, 2023.
Kellerman, A. M., Dittmar, T., Kothawala, D. N., and Tranvik, L. J.: Chemodiversity of dissolved organic matter in lakes driven by climate and hydrology, Nat Commun, 5, 3804, 2014.
Leles, S. G. and Levine, N. M.: Mechanistic constraints on the trade-off between photosynthesis and respiration in response to warming, Science Advances, 9, eadh8043, 2023.
Li, X., Wang, J., Lin, J., Yin, W., Shi, Y. Y., Wang, L., Xiao, H. B., Zhong, Z. M., Jiang, H., and Shi, Z. H.: Hysteresis analysis reveals dissolved carbon concentration – discharge relationships during and between storm events, Water Research, 226, 119220, 2022a.
Li, Y., Zhou, Y., Zhou, L., Zhang, Y., Xu, H., Jang, K.-S., Kothawala, D. N., Spencer, R. G. M., Jeppesen, E., Brookes, J. D., Davidson, T. A., and Wu, F.: Changes in Water Chemistry Associated with Rainstorm Events Increase Carbon Emissions from the Inflowing River Mouth of a Major Drinking Water Reservoir, Environ Sci Technol, 56, 16494-16505, 2022b.
Li, Y., Zhu, D., Niu, L., Zhang, W., Wang, L., Zhang, H., Zou, S., and Zhou, C.: Carbon-fixing bacteria in diverse groundwaters of karst area: Distribution patterns, ecological interactions, and driving factors, Water Research, 261, 121979, 2024.
Lindström, E. S. and Bergström, A.-K.: Influence of inlet bacteria on bacterioplankton assemblage composition in lakes of different hydraulic retention time, Limnology and Oceanography, 49, 125-136, 2004.
Liu, S., Butman, D. E., and Raymond, P. A.: Evaluating CO_2 calculation error from organic alkalinity and pH measurement error in low ionic strength freshwaters, Limnology and Oceanography: Methods, 18, 606-622, 2020.
Liu, Z., Dreybrodt, W., and Wang, H.: A new direction in effective accounting for the atmospheric CO_2 budget: Considering the combined action of carbonate dissolution, the global water cycle and photosynthetic uptake of DIC by aquatic organisms, Earth-Science Reviews, 99, 162-172, 2010.
Liu, Z., Macpherson, G. L., Groves, C., Martin, J. B., Yuan, D., and Zeng, S.: Large and active CO_2 uptake by coupled carbonate weathering, Earth-Science Reviews, 182, 42-49, 2018.
Maberly, S. C., Barker, P. A., Stott, A. W., and De Ville, M. M.: Catchment productivity controls CO_2 emissions from lakes, Nature Climate Change, 3, 391-394, 2013.
Mendonça, R., Müller, R. A., Clow, D., Verpoorter, C., Raymond, P., Tranvik, L. J., and Sobek, S.: Organic carbon burial in global lakes and reservoirs, Nat Commun, 8, 1694, 2017.
Monteith, D. T., Henrys, P. A., Hruška, J., de Wit, H. A., Krám, P., Moldan, F., Posch, M., Räike, A., Stoddard, J. L., Shilland, E. M., Pereira, M. G., and Evans, C. D.: Long-term rise in riverine dissolved organic carbon concentration is predicted by electrolyte solubility theory, Science Advances, 9, eade3491, 2023.

Mu, C., Mu, M., Wu, X., Jia, L., Fan, C., Peng, X., Ping, C.-L., Wu, Q., Xiao, C., and Liu, J.: High carbon emissions from thermokarst lakes and their determinants in the Tibet Plateau, Global Change Biol, 29, 2732-2745, 2023.
Ni, M., Liu, R., Luo, W., Pu, J., Wu, S., Wang, Z., Zhang, J., Wang, X., and Ma, Y.: A comprehensive conceptual framework for signaling in-lake CO_2 through dissolved organic matter, Water Research, 264, 122228, 2024.
Ni, M., Liu, R., Luo, W., Pu, J., Zhang, J., and Wang, X.: Unexpected shifts of dissolved carbon biogeochemistry caused by anthropogenic disturbances in karst rivers, Water Research, 247, 120744, 2023.
Ni, M., Ma, Y., Wang, Z., Wang, X., and Zhu, S.: A distinctive mode of dissolved organic carbon biodegradation in karst lakes and reservoirs: Evidence from trophic controls and compositional transformations, Journal of Cleaner Production, 368, 133217, 2022.
Ni, M. F., Li, S. Y., Luo, J. C., and Lu, X. X.: CO_2 partial pressure and CO_2 degassing in the Daning River of the upper Yangtze River, China, J Hydrol, 569, 483-494, 2019.
Ohno, T.: Fluorescence Inner-Filtering Correction for Determining the Humification Index of Dissolved Organic Matter, Environ Sci Technol, 36, 742-746, 2002.
Pi, X., Luo, Q., Feng, L., Xu, Y., Tang, J., Liang, X., Ma, E., Cheng, R., Fensholt, R., Brandt, M., Cai, X., Gibson, L., Liu, J., Zheng, C., Li, W., and Bryan, B. A.: Mapping global lake dynamics reveals the emerging roles of small lakes, Nat Commun, 13, 5777, 2022.
Raymond, P. A. and Hamilton, S. K.: Anthropogenic influences on riverine fluxes of dissolved inorganic carbon to the oceans, Limnology and Oceanography Letters, 3, 143-155, 2018.
Raymond, P. A., Hartmann, J., Lauerwald, R., Sobek, S., McDonald, C., Hoover, M., Butman, D., Striegl, R., Mayorga, E., Humborg, C., Kortelainen, P., Durr, H., Meybeck, M., Ciais, P., and Guth, P.: Global carbon dioxide emissions from inland waters, Nature, 503, 355-359, 2013.
Rehn, L., Sponseller, R. A., Laudon, H., and Wallin, M. B.: Long-term changes in dissolved inorganic carbon across boreal streams caused by altered hydrology, Limnology and Oceanography, 68, 409-423, 2023.
Rodríguez-Cardona, B. M., Houle, D., Couture, S., Lapierre, J.-F., and del Giorgio, P. A.: Long-term trends in carbon and color signal uneven browning and terrestrialization of northern lakes, Communications Earth & Environment, 4, 338, 2023.
Serikova, S., Pokrovsky, O. S., Laudon, H., Krickov, I. V., Lim, A. G., Manasypov, R. M., and Karlsson, J.: High carbon emissions from thermokarst lakes of Western Siberia, Nat Commun, 10, 1552, 2019.
Shangguan, Q., Payn, R. A., Hall Jr, R. O., Young, F. L., Valett, H. M., and DeGrandpre, M. D.: Divergent metabolism estimates from dissolved oxygen and inorganic carbon: Implications for river carbon cycling, Limnology and Oceanography, 69, 2211-2228, 2024.
Song, K., Wen, Z., Xu, Y., Yang, H., Lyu, L., Zhao, Y., Fang, C., Shang, Y., and Du, J.: Dissolved carbon in a large variety of lakes across five limnetic regions in China, Journal of Hydrology, 563, 143-154, 2018.
Sun, H., Han, C., Liu, Z., Wei, Y., Ma, S., Bao, Q., Zhang, Y., and Yan, H.: Nutrient limitations on primary productivity and phosphorus removal by biological carbon pumps in dammed karst rivers: Implications for eutrophication control, Journal of Hydrology, 607, 127480, 2022.
Sun, P. a., He, S., Yu, S., Pu, J., Yuan, Y., and Zhang, C.: Dynamics in riverine inorganic and organic carbon based on carbonate weathering coupled with aquatic photosynthesis in a karst

catchment, Southwest China, Water Research, 189, 116658, 2021.
Tranvik, L. J., Downing, J. A., Cotner, J. B., Loiselle, S. A., Striegl, R. G., Ballatore, T. J., Dillon, P., Finlay, K., Fortino, K., Knoll, L. B., Kortelainen, P., Kutser, T., Larsen, S. H. H., Laurion, I., Leech, D. M., McCallister, S. L., McKnight, D. M., Melack, J. M., Overholt, E. P., Porter, J. A., Prairie, Y. T., Renwick, W. H., Roland, F., Sherman, B., Schindler, D. W., Sobek, S., Tremblay, A., Vanni, M. J., Verschoor, A. M., von Wachenfeldt, E., and Weyhenmeyer, G. A.: Lakes and reservoirs as regulators of carbon cycling and climate, Limnology and Oceanography, 54, 2298–2314, 2009.
Tye, A. M., Williamson, J. L., Jarvie, H. P., Dise, N. B., Lapworth, D. J., Monteith, D., Sanders, R., Mayor, D. J., Bowes, M. J., Bowes, M., Burden, A., Callaghan, N., Farr, G., Felgate, S. L., Gibb, S., Gilbert, P. J., Hargreaves, G., Keenan, P., Kitidis, V., Jürgens, M. D., Martin, A., Mounteney, I., Nightingale, P. D., Gloria Pereira, M., Olszewska, J., Pickard, A., Rees, A. P., Spears, B., Stinchcombe, M., White, D., Williams, P., Worrall, F., and Evans, C. D.: Dissolved inorganic carbon export from rivers of Great Britain: Spatial distribution and potential catchment-scale controls, Journal of Hydrology, 615, 128677, 2022.
Wang, H., Zhang, Q.-w., Chen, G., Li, X., Wang, Q.-l., Gao, L., Wang, J., He, D., and Li, M.: The loss of dissolved organic matter from biological soil crust at various successional stages under rainfall of different intensities: Insights into the changes of molecular components at different rainfall stages, Water Research, 257, 121719, 2024.
Wang, W., Li, S.-L., Zhong, J., Slowinski, S., Li, S., Li, C., Su, J., Yi, Y., Dong, K., Xu, S., Van Cappellen, P., and Liu, C.-Q.: Carbonate mineral dissolution and photosynthesis-induced precipitation regulate inorganic carbon cycling along the karst river-reservoir continuum, SW China, Journal of Hydrology, 615, 128621, 2022.
Xi, N., Zhang, T., Zhao, W., Jia, Y., Fan, J., Li, R., Li, J., and Pu, J.: Metabolic processes drive spatio-temporal variations of carbon sink/source in a karst river, Environmental Research, 262, 119970, 2024.
Xia, F., Liu, Z., Zhao, M., Li, Q., Li, D., Cao, W., Zeng, C., Hu, Y., Chen, B., Bao, Q., Zhang, Y., He, Q., Lai, C., He, X., Ma, Z., Han, Y., and He, H.: High stability of autochthonous dissolved organic matter in karst aquatic ecosystems: Evidence from fluorescence, Water Research, 220, 118723, 2022.
Xu, H., Xiao, Q., Dai, Y., Chen, D., Zhang, C., Jiang, Y., and Xie, J.: Selected Bacteria Are Critical for Karst River Carbon Sequestration via Integrating Multi-omics and Hydrochemistry Data, Microbial Ecology, 86, 3043-3056, 2023.
Xu, Y. Y., Pierrot, D., and Cai, W. J.: Ocean carbonate system computation for anoxic waters using an updated CO_2SYS program, Mar Chem, 195, 90-93, 2017.
Yan, Z., Xin, Y., Zhong, X., Yi, Y., Li, P., Wang, Y., Zhou, Y., He, Y., He, C., Shi, Q., Xu, W., and He, D.: Evolution of dissolved organic nitrogen chemistry during transportation to the marginal sea: Insights from nitrogen isotope and molecular composition analyses, Water Research, 249, 120942, 2024.
Yi, Y., Zhong, J., Bao, H., Mostofa, K. M. G., Xu, S., Xiao, H.-Y., and Li, S.-L.: The impacts of reservoirs on the sources and transport of riverine organic carbon in the karst area: A multi-tracer study, Water Research, 194, 116933, 2021.
Yuan, Y., Liang, X., Li, Q., Deng, J., Zou, J., Li, G., Chen, G., Qin, W., and Dai, H.: Response of a source water quality through a heavy precipitation event: Nutrients, dissolved organic matter and

their DBPs formation, Journal of Cleaner Production, 453, 142273, 2024.
Zhang, W., Wang, W., Zhong, J., Chen, S., Yi, Y., Xu, X., Chen, S., and Li, S.-L.: Carbon sequestration and decreased CO_2 emission caused by biological carbon pump effect: Insights from diel hydrochemical variations in subtropical karst reservoirs, Journal of Hydrology, 632, 130909, 2024.
Zhao, R., Huang, S., Pu, J., He, Q., Wang, H., and Jiang, X.: Effects of rainfall on the karst-related carbon cycle due to carbonate rock weathering induced by H2SO4 and/or HNO3, Journal of Hydrology, 630, 130664, 2024.

Figures:

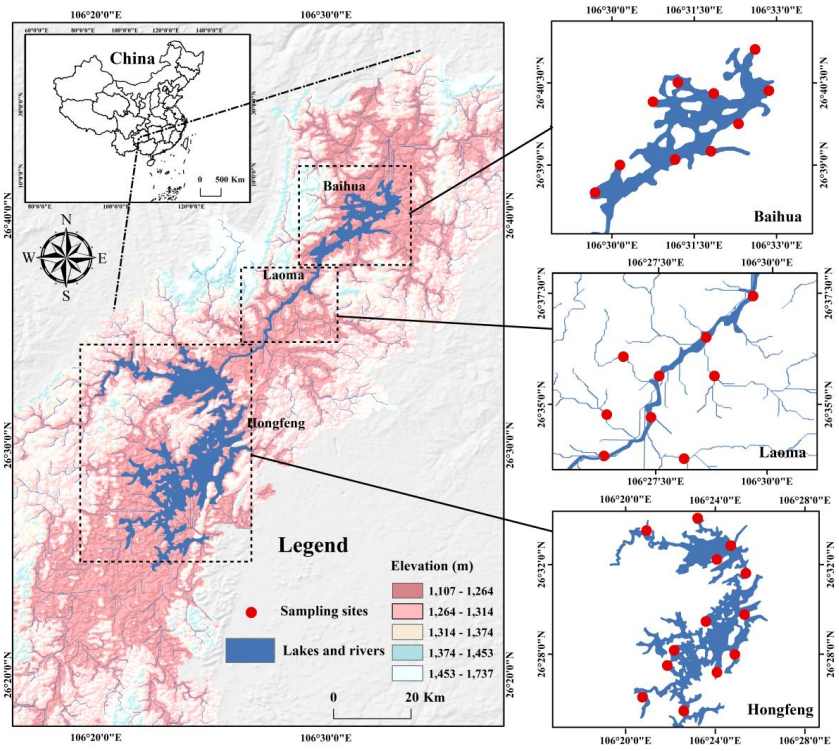

Fig. 1. Map showing DEM information and distribution of sampling locations in the karst lakes.

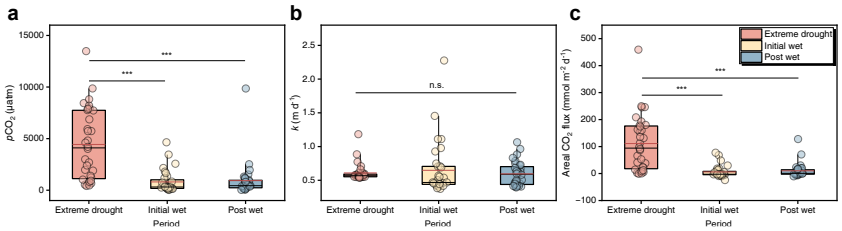

Fig. 2. Temporal patterns of pCO_2 (a), k (b) and areal CO_2 flux (c) across extreme drought, initial wet and post wet periods. The boxes with bars represent 25%–75% percentiles with 5%–95% percentiles. Black lines, white lines and dots show median, mean and all data, respectively. Asterisks indicate statistical significance: * $p < 0.05$, ** $p < 0.01$, *** $p < 0.001$; while n.s. indicates not significant ($p > 0.05$).

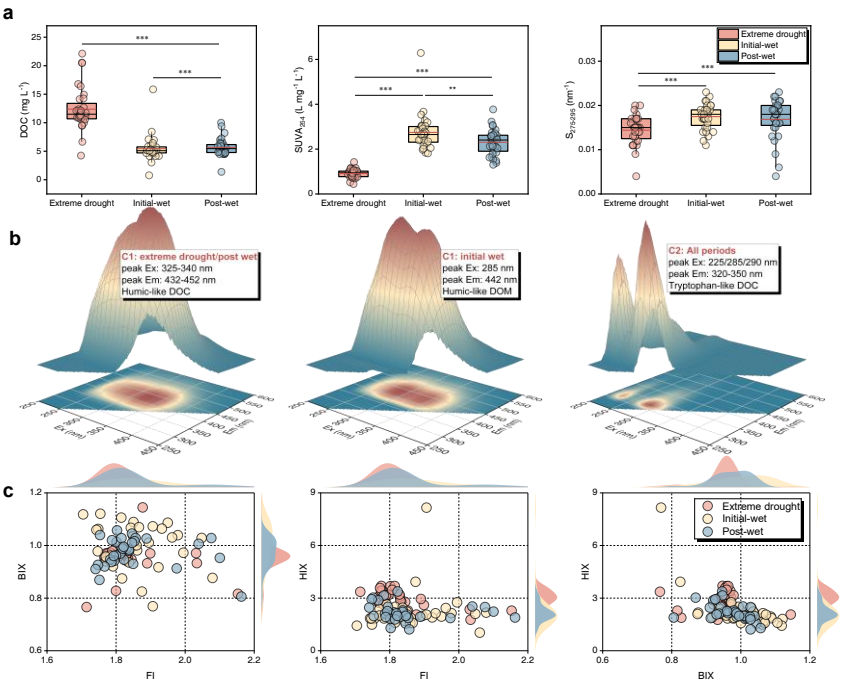

748

749 **Fig. 3.** Spectroscopic characteristics of DOC in the karst lakes. (a) Temporal patterns

750 of DOC, $SUVA_{254}$ and $S_{275-295}$ over the study periods. Symbols and lines follow the

751 same definitions as in Fig. 2. (b) 3D view of primary DOC fluorophores identified by

752 PARAFAC analysis. (c) Distributions of FI, BIX and HIX over the study periods.

753 Dots correspond to all data of these fluorescent parameters. The waves show Kernel

754 Smooth distributions of the data.

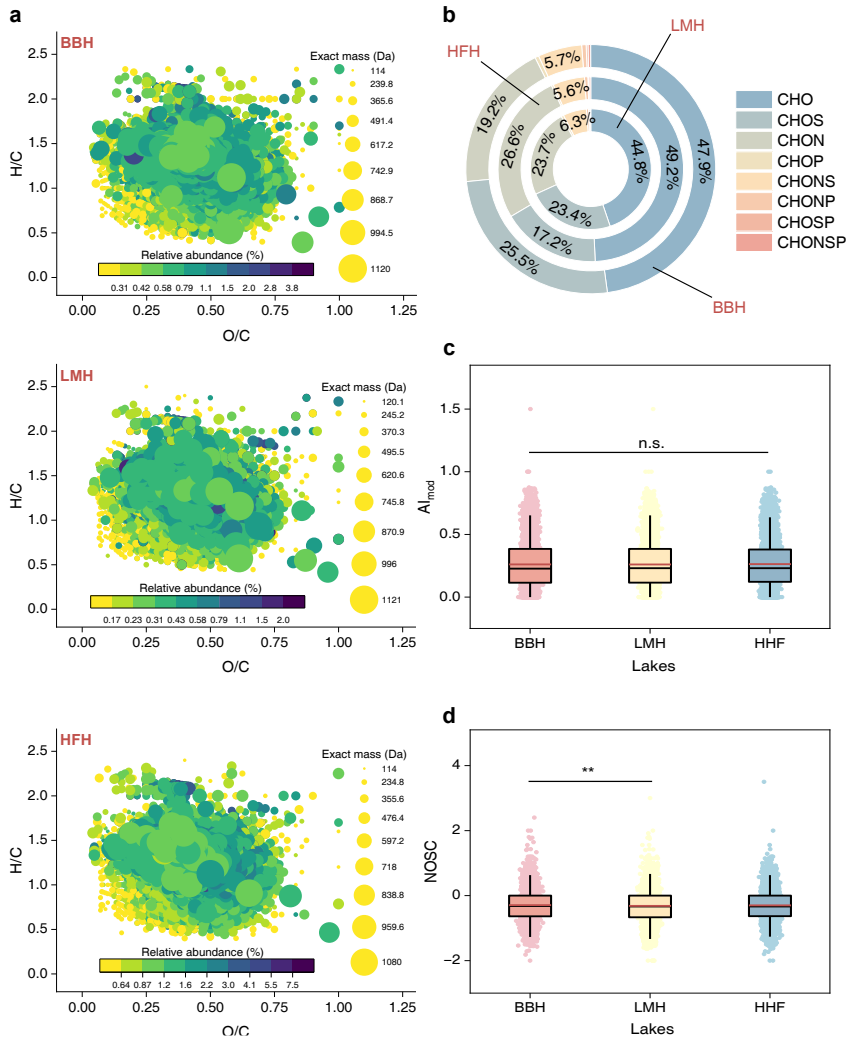

Fig. 4. Molecular characteristics of DOC in the karst lakes. (a) van Krevelen Diagrams plotting H/C against O/C with exact mass information of DOC molecules. (b) Proportions of primary DOC molecular formulas across the lakes. The AI-mod (c) and NOSC (d) across lakes. Symbols and lines follow the same definitions as in Fig. 2.

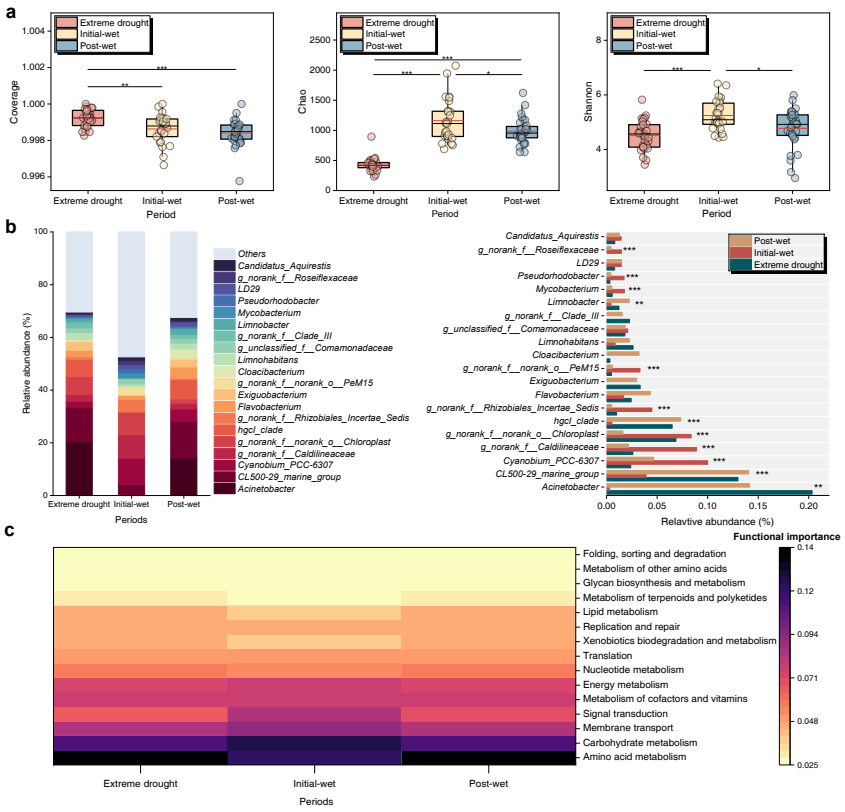

Fig. 5. Temporal variability of microbial communities and functions in the karst lakes. (a) Alpha diversity indices regarding Coverage, Chao and Shannon over the study periods. Symbols and lines follow the same definitions as in Fig. 2. (b) Comparison of the top 20 genera identified by relative abundance. (c) Potential microbial functions predicted by Tax4Fun based on the KEGG database.

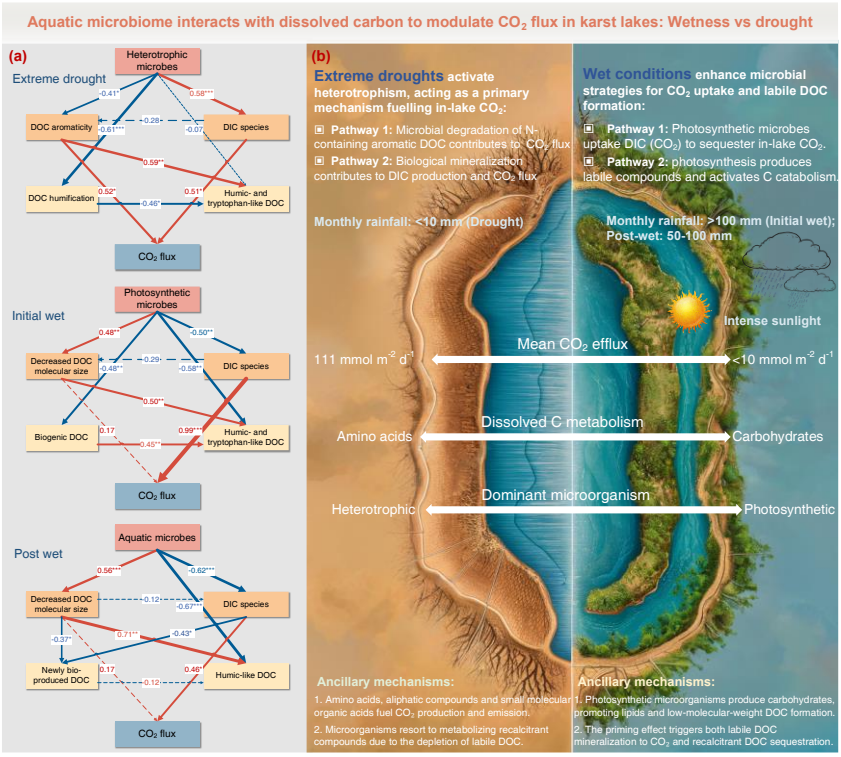

Fig. 6. Temporal pathways of aquatic microbiome-dissolved C interactions involved in CO_2 emission modulation in karst lakes. (a) The structural equation model showing temporal pathways of CO_2 flux driven by microbial communities and DIC-DOC turnover. Red and blue arrows represent positive and negative effects, respectively. Path coefficients are shown along the arrows. (b) A conceptual framework illustrating how microbiome interacts with dissolved carbon to modulate CO_2 emissions.

780 **Table 1.** Temporal patterns of pH, water temperature, total alkalinity and DIC species
781 in the karst lakes.

	n	Min	Max	Median	Mean	Std. Dev
Extreme drought						
pH	32	6.71	8.30	7.20	7.40	0.48
Water temperature (℃)	32	14.5	19.5	16.2	16.2	0.99
Total alkalinity (μeq L^{-1})	32	2325.7	4940.9	2726.5	2960.5	703.2
DIC (μmol L^{-1})	32	2405.0	5272.5	2828.5	3114.2	668.8
HCO_3^- (μmol L^{-1})	32	2290.3	4895.5	2645.1	2878.6	655.0
CO_3^{2-} (μmol L^{-1})	32	3.95	244.6	16.0	40.9	51.3
Dissolved CO_2 (μmol L^{-1})	32	18.0	602.4	177.0	194.7	153.5
Initial-wet						
pH	32	7.36	9.12	8.33	8.25	0.38
Water temperature (℃)	32	23.9	31.0	26.6	26.9	1.75
Total alkalinity (μeq L^{-1})	32	2178.7	6210.8	2895.3	3235.3	978.4
DIC (μmol L^{-1})	32	1538.7	6206.0	2688.8	3014.9	1042.5
HCO_3^- (μmol L^{-1})	32	918.4	5970.6	2428.0	2745.2	1073.0
CO_3^{2-} (μmol L^{-1})	32	35.7	752.7	218.2	243.5	155.1
Dissolved CO_2 (μmol L^{-1})	32	0.58	160.3	10.4	26.2	36.0
Post-wet						
pH	32	6.80	9.15	8.22	8.18	0.47
Water temperature (℃)	32	12.9	29.5	27.1	25.8	3.45
Total alkalinity (μeq L^{-1})	32	2239.7	5435.0	2795.5	3133.6	862.9
DIC (μmol L^{-1})	32	2096.8	5180.7	2576.5	2908.9	777.2
HCO_3^- (μmol L^{-1})	32	1546.7	4863.6	2441.5	2623.8	758.1
CO_3^{2-} (μmol L^{-1})	32	6.27	887.9	195.5	253.5	222.5
Dissolved CO_2 (μmol L^{-1})	32	1.04	315.9	14.3	31.6	57.1

782

783